Earth, Planets and Space

FULL PAPER

Open Access

CrossMark

Rupture features of the 2010 Mw 8.8 Chile earthquake extracted from surface waves

Yi-Ling Huang[1*], Ruey-Der Hwang[2], Yi-Shan Jhuang[1] and Cai-Yi Lin[2]

Abstract

This study used the rupture directivity theory to derive the fault parameters of the 2010 Mw 8.8 Chile earthquake on the basis of the azimuth-dependent source duration obtained from the Rayleigh-wave phase velocity. Results revealed that the 2010 Chile earthquake featured asymmetric bilateral faulting. The two rupture directions were N171°E (northward) and N17°E (southward), with rupture lengths of approximately 313 and 118 km, respectively, and were related to the locking degree in the source region. The entire source duration was approximately 187 s. After excluding the rise time from the source duration, the northward rupture velocity was approximately 2.02 km/s, faster than the southward rupture velocity (1.74 km/s). On average, the rupture velocity derived from this study was slower than that estimated from finite-fault inversion; however, several historical earthquakes in the Chile region also showed slow rupture velocity when using low-frequency signals, as surface waves do. Two earlier studies through global-positioning-system data analysis showed that the static stress drop of 50–70 bars for the 2010 Chile earthquake was higher than that for subduction-zone earthquakes. Hence, a remarkable feature was that the 2010 Chile earthquake had a slow rupture velocity and a high static stress drop, which suggested an inverse relationship between rupture velocity and static stress drop.

Keywords: 2010 Chile earthquake, Rupture velocity, Rise time, Static stress drop

Background

On February 27, 2010, the megathrust Chile earthquake (Mw 8.8) occurred near the coast of Maule in central Chile (Fig. 1). The earthquake generated a large rupture and caused severe damage along the coast and in nearby regions. Large earthquakes occurred frequently in the Chile region, where the Nazca plate subducts beneath the South American plate with a relative moving velocity of ~6.5 cm/year (Contreras-Reyes and Carrizo 2011). The most well-known event is the 1960 Mw 9.5 Chile earthquake, the largest event observed using modern seismic instruments. However, in the central and southern areas of Chile (35°S–37°S), no large events occurred during 1835–2010; consequently, the region was regarded as a zone with seismic gap (Ruegg et al. 2009; Moreno et al. 2010, 2012). Moreno et al. (2010)
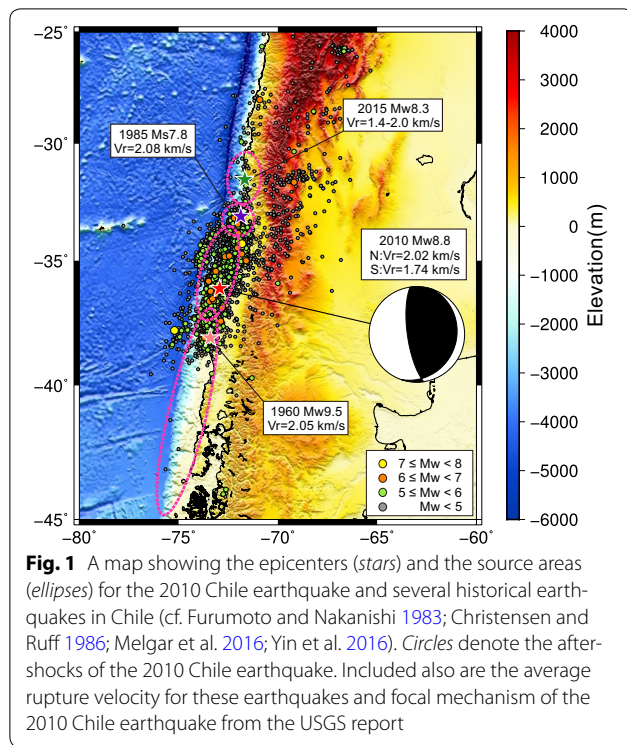
analyzed global positioning system (GPS) data and compared several source rupture models to suggest that the 2010 Chile earthquake occurs in the locked region, where no obvious displacements were observed prior to this event. The slip model from the joint inversion of GPS, interferometric synthetic aperture radar (InSAR), and land-level change data (Moreno et al. 2012) showed large slips related to the locked region, also consistent with the results of Vigny et al. (2011).

After the 2010 Chile earthquake, several studies used finite-fault inversion and P-wave back-projection analysis to probe the complex rupture process of the earthquake. Kiser and Ishii (2011) obtained a fast rupture velocity to the north and a slower one to the south, but Delouis et al. (2010) concluded contrarily. Furthermore, the average rupture velocity reported in previous studies varied widely from 2.0 to 3.2 km/s (Delouis et al. 2010; Lay et al. 2010; Kiser and Ishii 2011; Vigny et al. 2011; Wang and Mori 2011). Ruptures derived from different frequency contents also showed various rupture features through

*Correspondence: ylhuang@ntou.edu.tw
[1] Institute of Applied Geosciences, National Taiwan Ocean University, No.2, Beining Rd., Keelung 202, Taiwan, ROC
Full list of author information is available at the end of the article

Huang *et al. Earth, Planets and Space* (2017) 69:41

Page 2 of 8

Fig. 1 A map showing the epicenters (*stars*) and the source areas (*ellipses*) for the 2010 Chile earthquake and several historical earthquakes in Chile (cf. Furumoto and Nakanishi 1983; Christensen and Ruff 1986; Melgar et al. 2016; Yin et al. 2016). *Circles* denote the aftershocks of the 2010 Chile earthquake. Included also are the average rupture velocity for these earthquakes and focal mechanism of the 2010 Chile earthquake from the USGS report

P-wave back-projection analysis (e.g., Kiser and Ishii 2011; Wang and Mori 2011).

In previous studies, the rupture characteristics of the 2010 Chile earthquake were mainly inferred using source rupture models inverted from P-waves and GPS data. However, surface waves can also provide evidence for further understanding of the rupture features of large earthquakes (cf. Ben-Menahem 1961; Christensen and Ruff 1986; Zhang and Kanamori 1988; Velasco et al. 1994; Hwang et al. 2001; Ammon et al. 2006). In this study, Rayleigh-wave travel-time delays, caused by the source finiteness of the 2010 Chile earthquake, were used to estimate the fault parameters through rupture directivity analysis (e.g., Velasco et al. 1994; Hwang et al. 2001, 2011; Ammon et al. 2006; Chang et al. 2010; Hwang 2014).
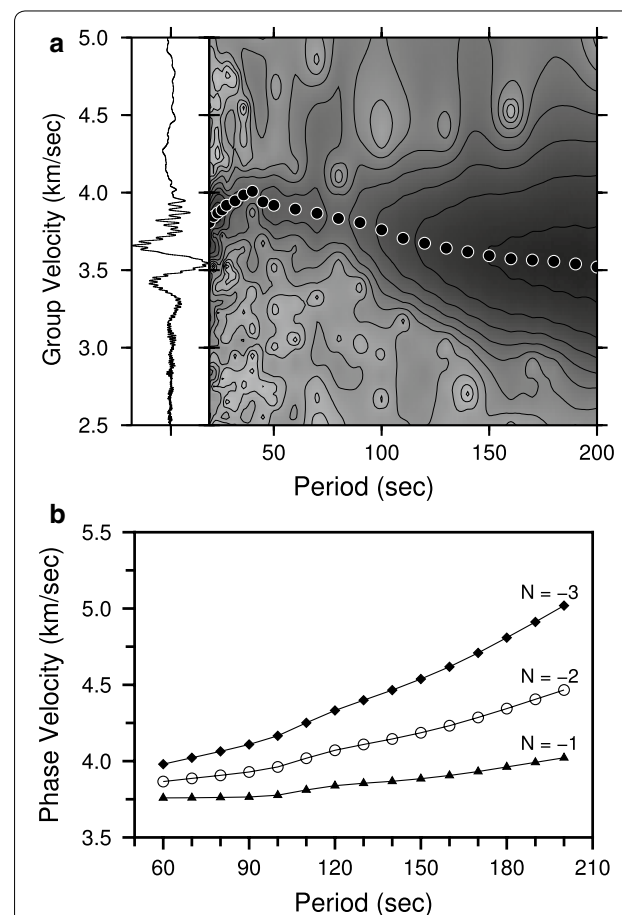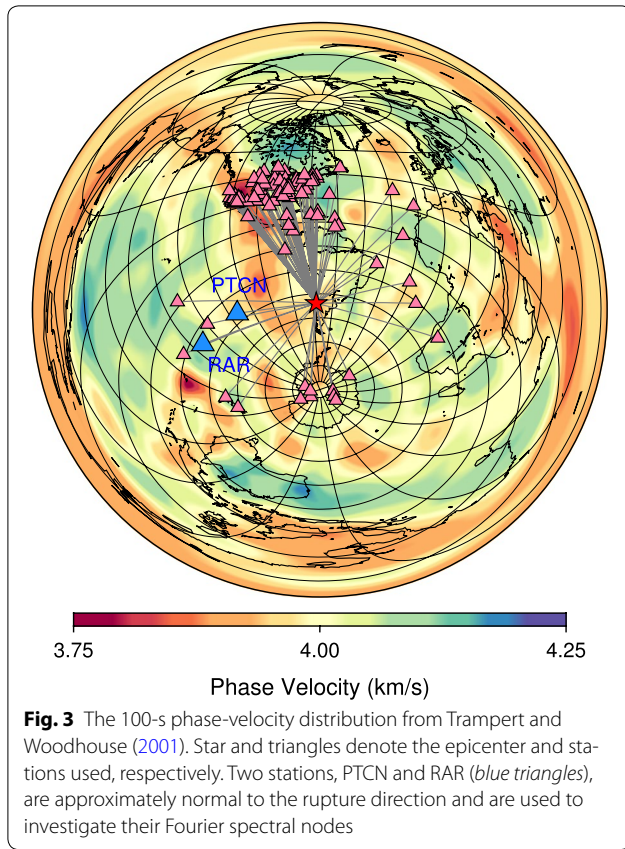
Data

Rayleigh waves generated by the 2010 Chile earthquake at epicentral distances of 30°–90° were used to calculate its corresponding travel times. After removing instrumental response, the Rayleigh waves were filtered between 0.004 and 0.2 Hz. To confirm whether seismograms were appropriate for phase-velocity calculation, we first used the multiple-filter technique (cf. Dziewonski et al. 1969; Herrmann 1973) to inspect Rayleigh-wave energy varying with periods. Hence, only data exhibiting strong Rayleigh-wave excitations with stable group-velocity dispersion curves were first selected for the follow-up

phase-velocity determination (Fig. 2a). Next, a single-station method was adopted to calculate the phase velocity as in Eq. (2). Figure 3 shows the station distribution and the 154 Rayleigh-wave ray path data used in this study.

Methods

A large earthquake always produces a large rupture and a long source duration, which increase the observed travel time of surface waves (cf. Hwang et al. 2001, 2011; Chang et al. 2010; Hwang 2014). Under the assumption that the rupture process is uniform and has a constant rupture velocity, the increasing travel time depends on the source duration and is half the source duration (e.g., Ben-Menahem 1961; Hwang 2014). Owing to the rupture directivity of the source, we would observe different source durations at various station azimuths. Azimuth-dependent source duration, also called apparent source duration,

Fig. 2 a An example of a group-velocity dispersion curve, determined using the multiple-filter technique (MFT). *Circles* represent the group velocity varying with periods. **b** After removing the initial phase, the phase velocity along the source-station path can be reasonably determined by selecting a correct *N*-value. For this example, when $N = -2$, the phase velocities (*circles*) obtain reasonable values

Huang *et al. Earth, Planets and Space* (2017) 69:41

Page 3 of 8

Fig. 3 The 100-s phase-velocity distribution from Trampert and Woodhouse (2001). Star and triangles denote the epicenter and stations used, respectively. Two stations, PTCN and RAR (*blue triangles*), are approximately normal to the rupture direction and are used to investigate their Fourier spectral nodes

can be used to derive the fault parameters for large earthquakes through rupture directivity analysis (e.g., Ben-Menahem 1961; Christensen and Ruff 1986; Zhang and Kanamori 1988; Velasco et al. 1994; Hwang et al. 2001, 2011; Hwang 2014). Therefore, the key to analyzing the rupture directivity of a large earthquake by using surface waves is to separate the apparent source duration from the surface-wave travel time observed at different stations.

Following Hwang et al. (2011) and Hwang (2014), a method for separating the apparent source duration from the observed travel time of surface wave (t_{surf}) is to calculate the theoretical travel time (t_{cal}), independent of the source and calculated from the global surface-wave phase-velocity maps of Trampert and Woodhouse (2001). When doubling the difference between t_{surf} and t_{cal} for each station, we can obtain the apparent source duration (T_{ASD}) varying with station azimuth below.

$$T_{ASD} = 2 \times (t_{surf} - t_{cal}) \tag{1}$$

Before acquiring T_{ASD}, we first calculated the observed phase velocity of Rayleigh waves from source to station using the single-station method (cf. Hwang and Yu 2005; Hwang 2014). Subsequently, the phase velocity was converted into the corresponding travel time as follows:

$$t_{surf}(T) = \frac{D}{C_R(T)} = (\Phi_{SR} - \Phi_{OR} \pm N)T = \Phi_{str}T + \frac{t_s}{2} \tag{2}$$

where $C_R(T)$ and $t_{surf}(T)$ denote the phase velocity and its corresponding travel time at period T; D is the epicentral distance; Φ_{SR} is the station phase after removing the instrumental response; Φ_{OR} is the initial phase of the source calculated using a known focal mechanism and the velocity structure in the source area (cf. Wang 1981); N is an arbitrary integer for modulating reasonable phase velocities of the long-period part (cf. Chang et al. 2010; Hwang 2014) (Fig. 2b); $\Phi_{str}T$ is the travel time of surface wave traveling purely through the structure; t_s is the source duration, corresponding to T_{ASD} in Eq. (1).

Trampert and Woodhouse (2001) provided a set of spherical harmonic coefficients with periods of 40, 60, 80, 100, and 150 s to reconstruct the global Rayleigh- and Love-wave phase-velocity maps. From these maps, we can optionally calculate the travel time between two points on the Earth's surface. The calculated travel time (t_{cal}) purely propagated along a great-circle path from a point to a point. Therefore, t_{cal}, independent of the source, was identical to $\Phi_{str}T$ in Eq. (2). Subtracting t_{cal} from t_{surf} acquired $\frac{t_s}{2}$, half the source duration.

In Eq. (1), T_{ASD} was related to the fault parameters, the rupture length (L), rupture velocity (V_r), and rise time of dislocation (τ). On the basis of the rupture directivity theory for an event with unilateral faulting (cf. Ben-Menahem 1961), T_{ASD} can be expressed in the following form:

$$T_{ASD} = \left(\frac{L}{V_r} + \tau\right) - \frac{L}{C}\cos\Theta = \left(\frac{L}{V_r} + \tau\right) - L\frac{\cos\Theta}{C} \tag{3}$$

where C is the phase velocity across the source area and $\cos\Theta$ is the angle between the station azimuth (ϕ_s) and rupture direction of the fault (ϕ_f). $\frac{L}{V_r}$ is the rupture time.

From Eq. (3), T_{ASD} had a linear relationship with $\cos\Theta$. When searching for a series of ϕ_f, we obtained an optimal ϕ_f under the condition that an optimal linear between T_{ASD} and $\cos\Theta$ with minimum misfit existed. The misfit was defined as in misfit $= 1 + \gamma$, where γ is cross-correlation coefficient. The slope, $\frac{L}{C}$ in Eq. (3), was then used to determine the rupture length when giving a known C. Moreover, the intercept, $\frac{L}{V_r} + \tau$, is the average source duration consisting of the rupture time and rise time. In Eq. (3), T_{ASD} and C are functions of period T, so Eq. (3) is used at a specified period. However, when the phase velocity C across the source area was known for each used period, Eq. (3) can lead to a linear relationship between T_{ASD} and $\frac{\cos\Theta}{C}$. Consequently, the rupture directivity analysis can be performed by simultaneously using
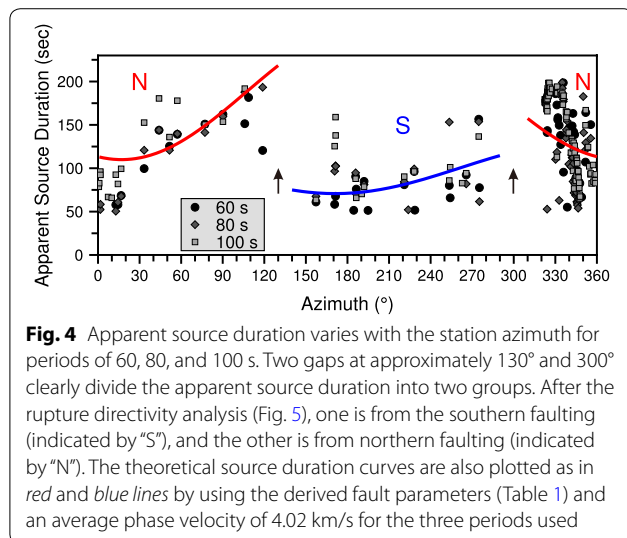
Huang *et al. Earth, Planets and Space* (2017) 69:41

Page 4 of 8

T_{ASD} observed from various periods. From the global phase velocity maps of Trampert and Woodhouse ([2001](#)), the phase velocities across the source area are 3.97, 4.00, and 4.10 km/s for periods of 60, 80, and 100 s, respectively. An average phase velocity is about 4.02 km/s.
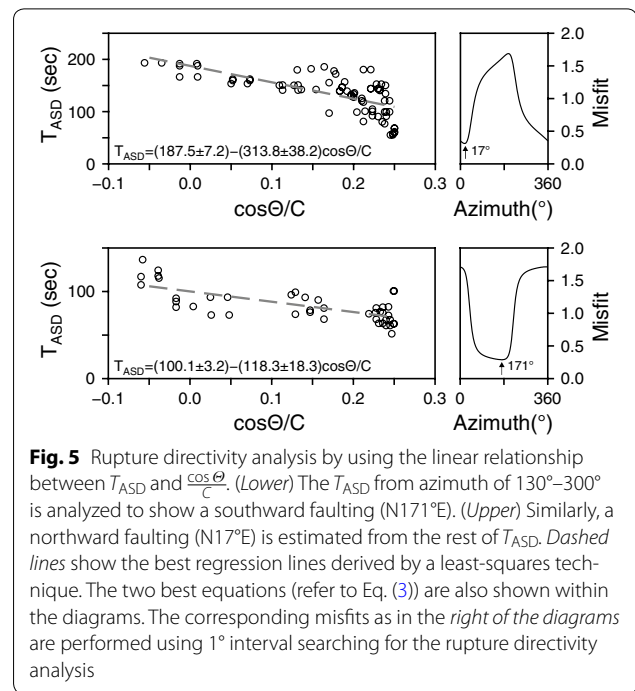
Results and discussion

Rupture directivity analysis

Figure [4](#) shows the apparent source duration determined from periods of 60, 80, and 100 s, respectively. Overall, distribution of the apparent source duration to station azimuth was uniform. Azimuths at approximately 130° and 300° divided these apparent source durations into two groups. Therefore, the apparent source duration varying with station azimuth indicated preliminarily the rupture feature of the 2010 Chile earthquake—not a unilateral faulting but a bilateral faulting [also refer to Figure 3 of Hwang ([2014](#))]. Because the 2010 Chile earthquake was an event with bilateral faulting, each of the two ruptures was considered a unilateral faulting and can be analyzed using Eq. ([3](#)). To stabilize rupture directivity analysis, we averaged the apparent source duration per 10° azimuth with a 5° moving window. Figure [5](#) shows the rupture directivity analysis of the T_{ASD} at azimuth of 130°–300° (Fig. [4](#)) performing the optimal linear equation, $T_{ASD} = (100.1 \pm 3.2) - (118.3 \pm 18.3)\frac{\cos\Theta}{C}$, with an optimal rupture azimuth of N171°E by a least-squares method. This denotes clearly the rupture that occurred toward the south along the fault. The rest of T_{ASD} was used to derive the other rupture, in which there was an optimal linear equation, $T_{ASD} = (187.5 \pm 7.2) - (313.8 \pm 38.2)\frac{\cos\Theta}{C}$, with an optimal rupture azimuth of N17°E; that is, the rupture was northward. The rupture to the north (N17°E) had a

Fig. 5 Rupture directivity analysis by using the linear relationship between T_{ASD} and $\frac{\cos\Theta}{C}$. (*Lower*) The T_{ASD} from azimuth of 130°–300° is analyzed to show a southward faulting (N171°E). (*Upper*) Similarly, a northward faulting (N17°E) is estimated from the rest of T_{ASD}. *Dashed lines* show the best regression lines derived by a least-squares technique. The two best equations (refer to Eq. ([3](#))) are also shown within the diagrams. The corresponding misfits as in the *right of the diagrams* are performed using 1° interval searching for the rupture directivity analysis

rupture length of approximately 313 km and exhibited the source duration of approximately 187 s, and thus, an average rupture velocity of 1.67 km/s was determined. However, the rupture to the south (N171°E) showed a rupture length of approximately 118 km with the source duration of approximately 100 s, and thus, an average rupture velocity was 1.18 km/s. Hence, the entire rupture length was about 430 km, including rupture length to the north and to the south. In this study, we assumed that the ruptures with uniform faulting occurred simultaneously toward the north and the south along the fault; hence, the source duration from the northern fault was regarded as the entire source duration of approximately 187 s. Here, because we used 100-s Rayleigh wave with the phase velocity of 4.10 km/s to detect the rupture length, its wavelength was 410 km, longer than the two rupture lengths derived as in Fig. [5](#). In terms of physics, the structure could be resolved when the size of the structure is larger than 1/4–1/8 wavelength of the signal used (cf. Fowler [2005](#)). For this reason, these periods used in our study were appropriate to investigate the rupture size of the 2010 Chile earthquake. Table [1](#) lists these fault parameters of the 2010 Chile earthquake determined from the rupture directivity analysis. Also, the predicated curves (theoretical azimuth-dependent source duration) calculated from the derived fault parameters (Table [1](#)) are displayed in Fig. [4](#).

The aforementioned results show that the rupture velocity of southward faulting is lower than that of northward faulting; furthermore, the rupture length and source

Fig. 4 Apparent source duration varies with the station azimuth for periods of 60, 80, and 100 s. Two gaps at approximately 130° and 300° clearly divide the apparent source duration into two groups. After the rupture directivity analysis (Fig. [5](#)), one is from the southern faulting (indicated by "S"), and the other is from northern faulting (indicated by "N"). The theoretical source duration curves are also plotted as in *red* and *blue lines* by using the derived fault parameters (Table [1](#)) and an average phase velocity of 4.02 km/s for the three periods used

Huang *et al. Earth, Planets and Space* (2017) 69:41

Page 5 of 8

Table 1 Fault parameters estimated from 60-, 80-, and 100-s Rayleigh waves in this study

Fault parameters	Northern segment	Southern segment
Rupture length (km)	313	118
Source duration (s)	187	100
Rupture azimuth (°)[a]	17	171
Rise time (s)	32.3	
Rupture velocity (km/s)[b]	1.67	1.18
Rupture velocity (km/s)[c]	2.02	1.74

[a] Rupture azimuth is estimated clockwise from the north

[b] Rupture velocity is calculated from the average source duration

[c] Rupture velocity is calculated after deducting the rise time from the average source duration

duration in the southern fault are also shorter than those in the northern one. Moreno et al. (2012) stated that the larger slip distribution of the 2010 Chile earthquake is consistent with those areas with a larger locking degree on the fault. As displayed in Fig. 6, the rupture directions for the two ruptures are N17°E and N171°E, which corresponds to the distribution of a larger locking degree ($\geq$0.75) on the fault (Moreno et al. 2012). That is, the ruptures occur along the areas with a larger locking degree, in which the Poisson's ratios are also relatively lower (e.g., Hicks et al. 2014; Moreno et al. 2014). Evidently, the rupture features of the 2010 Chile earthquake closely correlate with the structures of the source area. Additionally, the rupture length to the south is not as long as that to the north, probably because the southern rupture overlaps the slips of the 1960 Mw 9.5 Chile earthquake, which released stress previously so that the rupture to the south is prevented (Fig. 1). The source duration (187 s) from this study is relatively longer than that (110–160 s) from several finite-fault sources (e.g., Delouis et al. 2010; Lay et al. 2010; Sladen et al. 2010), but comparable with that (195 s) determined from an empirical relationship between seismic moment and source duration (Furumoto and Nakanishi 1983) by using a seismic moment of 1.86×10^{22} Nm (reported from Global CMT). This is likely because we use long-period signals to estimate the fault parameters, whereas the fault parameters are derived from finite-fault source using short-period ones. Kiser and Ishii (2011) and Wang and Mori (2011) have also reported different rupture features when using various frequency-content signals.

Rupture velocity and rise time

The rupture velocities were initially estimated at 1.67 km/s for the northern rupture and 1.18 km/s for the southern one from the entire source duration, containing the rupture time and rise time (Eq. (3)). Hence, these
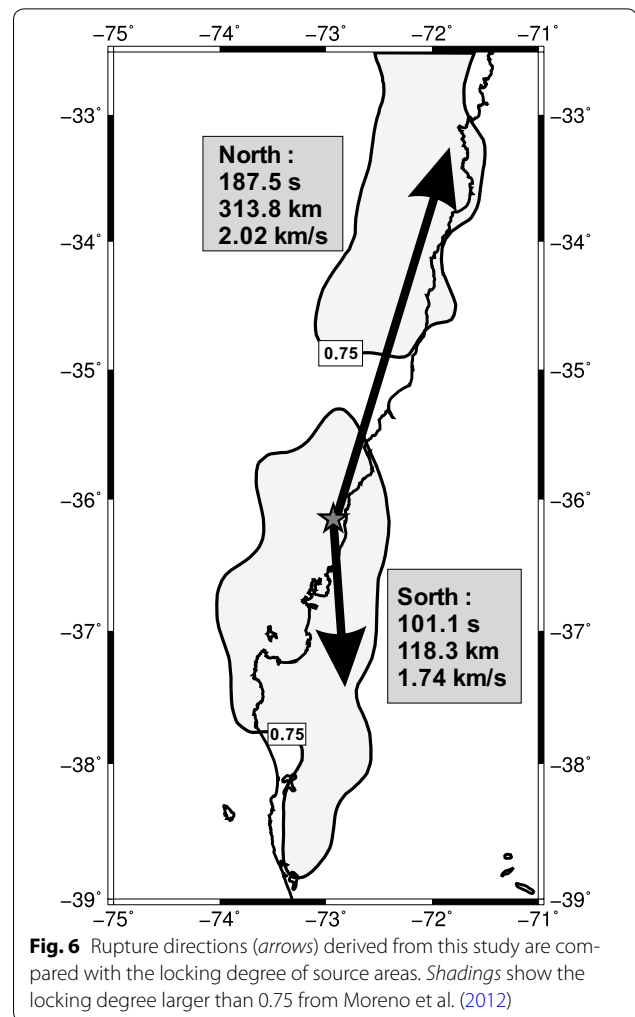

Fig. 6 Rupture directions (*arrows*) derived from this study are compared with the locking degree of source areas. *Shadings* show the locking degree larger than 0.75 from Moreno et al. (2012)

two rupture velocities are underestimated because we did not exclude the rise time from the entire source duration for the two ruptures. In Eq. (3), the apparent source time includes three components: rupture time ($\frac{L}{V_r}$); rise time (τ); ($\frac{L}{C} \cos \Theta$), which is created from rupture directivity along the rupture length. However, separating the rise time from the apparent source duration in the time domain is difficult. Here, following Hwang et al. (2011), we first selected the stations approximately normal to the rupture directivity; then, $\frac{L}{C} \cos \Theta$ vanished because of $\Theta = 90°$, and the apparent source time is $\frac{L}{V_r} + \tau$. This would make the analysis simplified for separating the rise time from the entire source duration. In the time domain, the rupture time and rise time increase the travel time of surface waves, whereas in the frequency domain, the rupture time and rise time all represent sinc functions that produce many nodes in the surface-wave Fourier spectra. Hence, these periods of nodes can be used to indicate rupture time and rise time. In general, the rise time

Huang *et al. Earth, Planets and Space* (2017) 69:41

Page 6 of 8

is about 0.10–0.25 times smaller than the rupture time (cf. Geller 1976; Heaton 1990) so that the period of node created from the rupture time is relatively easier to be inspected than that from the rise time. From the Fourier spectra influenced by the sinc functions, the rupture time is a multiple of the period of the node (cf. Chang et al. 2010; Hwang et al. 2001, 2011). Moreover, the longest period among nodes, the first node, directly denotes the rupture time.

From Hwang (2014), for a bilateral rupture analyzed by surface-wave travel time, the stations received the surface waves from the minor travel-time component rather than from the longer travel-time one. According to the concepts, five criteria were used to choose appropriate stations for the follow-up spectral analysis: (1) These stations were approximately perpendicular to the rupture direction of the southern faulting that produces the minor travel time relative to the northern one; (2) the apparent source duration for the two stations corresponded to the source duration (~100 s) of the southern rupture because $\frac{L}{C}\cos\Theta$ disappears; (3) there are clear spectral nodes in these stations used; (4) the period of the first spectral node is shorter than the apparent source duration; (5) the difference between first spectral-node period and apparent source duration is about 0.1–0.2 times the entire source duration (cf. Geller 1976; Heaton 1990). Finally, we selected stations PTCN and RAR for completing the spectral analysis to further evaluate the rise time (Figs. 3, 7).

Figure 7 shows the Fourier spectra of stations PTCN and RAR. For station PTCN, the first-node period was 60.2 s, which are subtracted from its apparent source duration (94.2 s) to yield a rise time of 34.0 s. Similarly, the rise time was estimated at 30.5 s from station RAR. For an earthquake rupture, the rise is constant and does not vary with station azimuth. Hence, here, we averaged the two rise times as 32.3 s. Since the rise time for the 2010 Chile earthquake was drawn from the Fourier spectral analysis, we recalculated the rupture velocity to be 2.02 km/s for the northern rupture and 1.74 km/s for the southern one after deducting the rise time from their source duration, respectively. On average, the rupture velocity for the 2010 Chile earthquake from this study is still lower than that from source rupture inversion (e.g., Delouis et al. 2010; Lay et al. 2010; Vigny et al. 2011), but it is comparable with the 1992 Nicaragua earthquake (cf. Kikuchi and Kanamori 1995) and the 2011 Tohoku earthquake (cf. Hwang 2014), which were events with bilateral faulting and low rupture velocity. Nevertheless, that the rupture velocity in the northern faulting is faster than that in the southern one is also consistent with the result of Kiser and Ishii (2011) from P-wave back-projection analysis.
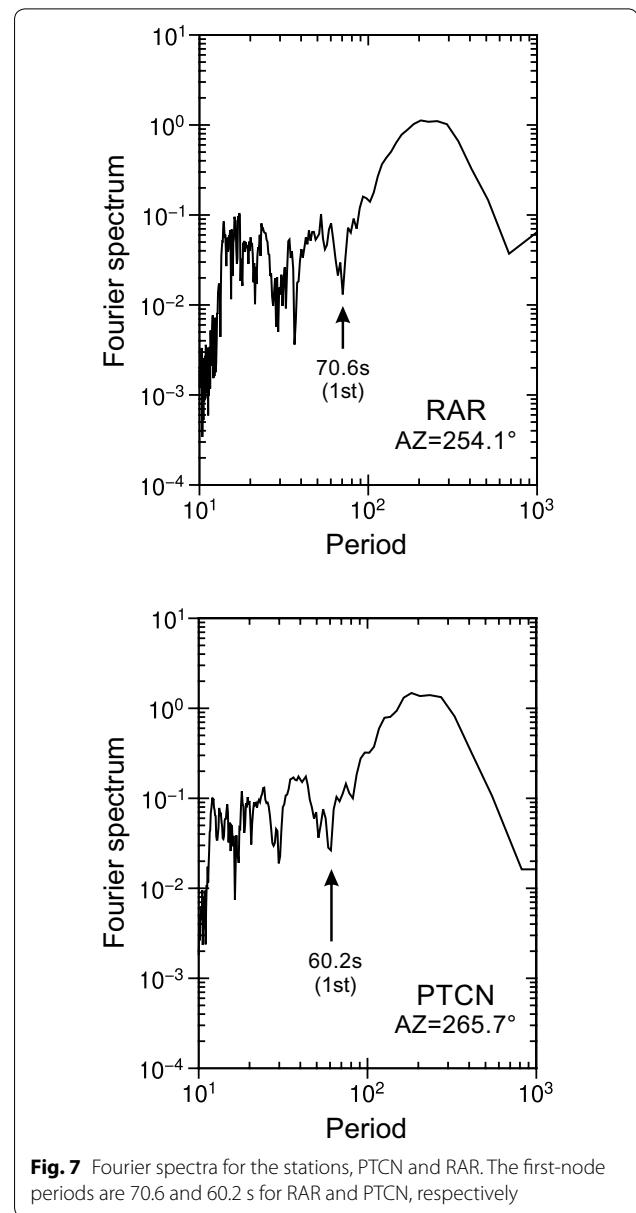
Fig. 7 Fourier spectra for the stations, PTCN and RAR. The first-node periods are 70.6 and 60.2 s for RAR and PTCN, respectively

As in Fig. 1, several large earthquakes once occurred in the subduction zone, where the Nazca plate subducts under the South American plate. The 2010 Chile earthquake compensated the seismic gap between the 1960 Mw 9.5 Chile earthquake and the 1985 Ms 7.8 earthquake (Ruegg et al. 2009). Previous studies revealed that the 1960 Mw 9.5 Chile earthquake and the 1985 Ms 7.8 earthquake have the average rupture velocity of 2.05 and 2.08 km/s from surface-wave analysis (cf. Furumoto and Nakanishi 1983; Christensen and Ruff 1986). Yin et al. (2016) used compressive sensing (CS) method by using P-waves with frequencies of 0.05–0.5 Hz to derive an average rupture velocity of 1.4 km/s, which also low

Huang *et al. Earth, Planets and Space* (2017) 69:41

Page 7 of 8

as also reported by Melgar et al. (2016) in 2.0 km/s. In other words, these earthquakes occurring in the Chile region all show low rupture velocity, as analyzed from low-frequency signals (Fig. 1). In addition, the 2010 Mw 8.8 Chile earthquake exhibited high static stress drop of 50–70 bars (Luttrell et al. 2011; Wang et al. 2015), relatively larger than earthquakes (30 bars) in the subduction zone (cf. Kanamori and Anderson 1975). That is, the 2010 Chile earthquake is an event with a low rupture velocity and a high static stress drop. This is similar to the analysis of the 2011 Tohoku earthquake, which is also a bilateral rupture event (Hwang 2014). Such results imply an inverse relationship between static stress drop and rupture velocity as addressed by Kanamori and Rivera (2004). Several studies also support the inverse relationship (e.g., Tan and Helmberger 2010; Hwang et al. 2012; Causse and Song 2015).

Conclusions

The rupture directivity analysis by using phase velocities with periods of 60, 80, and 100 s revealed that the 2010 Chile earthquake could be characterized by the following: (1) The earthquake was an asymmetric bilateral faulting event. (2) Two rupture directions were N17°E toward the north and N171°E toward the south, respectively. (3) The rupture length, source duration, and rupture velocity of the northern segment were all larger than those of the southern segment. (4) The rise time of approximately 32.3 s was about 0.17 times of the source duration (187 s), agreeing with the proposal of Geller (1976) and Heaton (1990). As mentioned earlier, the rupture features for the 2010 Chile earthquake from this study were consistent with the locking degree in the source area (Moreno et al. 2012), which indicated the seismogenic structures controlling the earthquake rupture process. Additionally, the low rupture velocity and high static stress drop for the 2010 Chile earthquake seemed to support the inverse relationship between these parameters, as reported by Kanamori and Rivera (2004).

Authors' contributions

YL drafted the manuscript. RD revised the manuscript and drafted the part of the manuscript. YS analyzed seismic data. CI drew all figures. All authors read and approved the final manuscript.

Author details

[1] Institute of Applied Geosciences, National Taiwan Ocean University, No.2, Beining Rd., Keelung 202, Taiwan, ROC. [2] Department of Geology, Chinese Culture University, No.55, Hwa-Kang Rd., Yang-Ming-Shan, Taipei 111, Taiwan, ROC.

References

Ammon CJ, Velasco AA, Lay T (2006) Rapid estimation of first-order rupture characteristics for large earthquakes using surface waves: 2004 Sumatra-Andaman earthquake. Geophys Res Lett 33:L14314. doi:10.1029/2006GL026303

Ben-Menahem A (1961) Radiation of seismic surface-waves from finite moving sources. Bull Seismol Soc Am 51:401–435

Causse M, Song SG (2015) Are stress drop and rupture velocity of earthquakes independent? Insight from observed ground motion variability. Geophys Res Lett 42:7383–7389

Chang JP, Hwang RD, Wang CY, Yu GK, Chang WY, Lin TW (2010) Analysis of rupture directivity for the 2004 Sumatra earthquake from the Rayleigh-wave phase velocity. Terr Atmos Ocean Sci 21:243–251. doi:10.3319/TAO.2009.03.27.01(T)

Christensen DH, Ruff LJ (1986) Rupture process of the March 3, 1985 Chilean earthquake. Geophys Res Lett 13:721–724

Contreras-Reyes E, Carrizo D (2011) Control of high oceanic features and subduction channel on earthquake ruptures along the Chile–Peru subduction zone. Phys Earth Planet Inter 186:49–58

Delouis B, Nocquet JM, Vallée M (2010) Slip distribution of the February 27, 2010 Mw = 8.8 Maule earthquake, central Chile, from static and high-rate GPS, InSAR, and broadband teleseismic data. Geophys Res Lett 37:L17305. doi:10.1029/2010GL043899

Dziewonski A, Bloch S, Landisman M (1969) A technique for the analysis of transient seismic signals. Bull Seismol Soc Am 59:427–444

Fowler CMR (2005) The solid earth: an introduction to global geophysics, 2nd edn. Cambridge University Press, Cambridge

Furumoto M, Nakanishi I (1983) Source times and scaling relations of large earthquakes. J Geophys Res 88:2191–2198

Geller RJ (1976) Scaling relations for earthquake source parameters and magnitudes. Bull Seismol Soc Am 66:1501–1523

Heaton TH (1990) Evidence for and implications of self-healing pulses of slip in earthquake rupture. Phys Earth Planet Inter 64:1–20

Herrmann RB (1973) Some aspects of band-pass filtering of surface waves. Bull Seismol Soc Am 63(2):663–671

Hicks SP, Rietbrock A, Ryder IMA, Lee CS, Miller M (2014) Anatomy of a megathrust: the 2010 M8.8 Maule, Chile earthquake rupture zone imaged using seismic tomography. Earth Planet Sci Lett 405:142–155

Hwang RD (2014) First-order rupture features of the 2011 MW 9.0 Tohoku (Japan) earthquake from surface waves. J Asian Earth Sci 81:20–27

Hwang RD, Yu GK (2005) Shear-wave velocity structure of upper mantle under Taiwan from the array analysis of surface waves. Geophys Res Lett 32:L07310. doi:10.1029/2004GL021868

Hwang RD, Yu GK, Wang JH (2001) Rupture directivity and source-process time of the September 20, 1999 Chi-Chi, Taiwan, earthquake estimated from Rayleigh-wave phase velocity. Earth Planets Space 53(12):1171–1176. doi:10.1186/BF03352412

Hwang RD, Chang JP, Wang CY, Wu JJ, Kuo CH, Tsai YW, Chang WY (2011) Rise time and source duration of the 2008 Mw 7.9 Wenchuan (China) earthquake as revealed by Rayleigh-waves. Earth Planets Space 63:427–434. doi:10.5047/eps.2011.01.002

Hwang R-D, Lin T-W, Wu C-C, Chang W-Y, Chang J-P (2012) Reexamining the source parameters of the 2010 M_L 6.4 JiaSian (Taiwan) earthquake using the inversion of teleseismic *P*-waves. J Asian Earth Sci 48:24–30

Kanamori H, Anderson DL (1975) Theoretical basis of some empirical relations in seismology. Bull Seismol Soc Am 65:1073–1095

Kanamori H, Rivera L (2004) Static and dynamic scaling relations for earthquakes and their implications for rupture speed and stress drop. Bull Seismol Soc Am 94:314–319

Kikuchi M, Kanamori H (1995) Source characteristics of the 1992 Nicaragua tsunami earthquake inferred from teleseismic body waves. Pure Appl Geophys 144:441–453

Huang *et al. Earth, Planets and Space* (2017) 69:41

Page 8 of 8

Kiser E, Ishii M (2011) The 2010 Mw 8.8 Chile earthquake: triggering on multiple segments and frequency-dependent rupture behavior. Geophys Res Lett 38:L07301. doi:10.1029/2011GL047140

Lay T, Ammon C, Kanamori H, Koper K, Sufri O, Hutko A (2010) Teleseismic inversion for rupture process of the 27 February 2010 Chile (Mw 8.8) earthquake. Geophys Res Lett 37:L13301. doi:10.1029/2010GL043379

Luttrell KM, Tong X, Sandwell DT, Brooks BA, Bevis MG (2011) Estimates of stress drop and crustal tectonic stress from the 27 February 2010 Maule, Chile, earthquake: implications for fault strength. J Geophys Res 116:B11401. doi:10.1029/2011JB008509

Melgar D, Fan W, Riquelme S, Geng J, Liang C, Fuentes M, Vargas G, Allen RM, Shearer PM, Fielding EJ (2016) Slip segmentation and slow rupture to the trench during the 2015, Mw 8.3 Illapel, Chile earthquake. Geophys Res Lett 3:961–966. doi:10.1002/2015GL067369

Moreno M, Rosenau M, Oncken O (2010) 2010 Maule earthquake slip correlates with pre-seismic locking of Andean subduction zone. Nature 467:198–202

Moreno M, Melnick D, Rosenau M, Baez J, Klotz J, Oncken O, Tassara A, Chen J, Bataille K, Bevis M, Socquet A, Bolte J, Vigny C, Brooks B, Ryder I, Grund V, Smalley B, Carrizo D, Bartsch M, Hase H (2012) Toward understanding tectonic control on the Mw 8.8 2010 Maule Chile earthquake. Earth Planet Sci Lett 321:152–165

Moreno M, Haberland C, Oncken O, Rietbrock A, Angiboust S, Heidbach O (2014) Locking of the Chile subduction zone controlled by fluid pressure before the 2010 earthquake. Nat Geosci 7:292–296

Ruegg J, Rudloff A, Vigny C, Madariaga R, De Chabalier J, Campos J, Kausel E, Barrientos S, Dimitrov D (2009) Interseismic strain accumulation measured by GPS in the seismic gap between Constitución and Concepción in Chile. Phys Earth Planet Inter 175:78–85

Sladen A, Simons M, Bevis M, Brooks B, Foster J, Smalley J, Owen S (2010) A coseismic distributed slip model for the 2010 Mw 8.8 Maule (Chile)

earthquake. In: Paper presented at the giant earthquakes and their tsunamis, AGU Chapman conference, Abstract

Tan Y, Helmberger D (2010) Rupture directivity characteristics of the 2003 Big Bear sequence. Bull Seismol Soc Am 100:1089–1106

Trampert J, Woodhouse JH (2001) Assessment of global phase velocity models. Geophys J Inter 144:165–174

Velasco AA, Ammon CJ, Lay T, Zhang J (1994) Imaging a slow bilateral rupture with broadband seismic waves: the September 2, 1992 Nicaraguan tsunami earthquake. Geophys Res Lett 21:2629–2632. doi:10.1029/94GL02402

Vigny C, Socquet A, Peyrat S, Ruegg JC, Métois M, Madariaga R, Morvan S, Lancieri M, Lacassin R, Campos J, Carrizo D, Bejar-Pizarro M, Barrientos S, Armijo R, Aranda C, Valderas-Bermejo MC, Ortega I, Bondoux F, Baize S, Lyon-Caen H, Pavez A, Vilotte JP, Bevis M, Brooks B, Smalley R, Parra H, Baez JC, Blanco M, Cimbaro S, Kendrick E (2011) The 2010 Mw 8.8 Maule megathrust earthquake of Central Chile, monitored by GPS. Science 332:1417–1421

Wang CY (1981) Wave theory for seismogram synthesis. Ph.D. Dissertation, Saint Louis University, Saint Louis, 235 pp

Wang D, Mori J (2011) Frequency-dependent energy radiation and fault coupling for the 2010 Mw 8. 8 Maule, Chile, and 2011 Mw 9. 0 Tohoku, Japan, earthquakes. Geophys Res Lett 38:L2230. doi:10.1029/2011GL049652

Wang L, Zöller G, Hainzl S (2015) Joint determination of slip and stress drop in a Bayesian inversion approach: a case study for the 2010 M8.8 Maule earthquake. Pure Appl Geophys 172:375–388

Yin J, Yang H, Yao H, Weng H (2016) Coseismic radiation and stress drop during the 2015 M_W 8.3 Illapel, Chile megathrust earthquake. Geophys Res Lett 43:1520–1528. doi:10.1002/2015GL067381

Zhang J, Kanamori H (1988) Source finiteness of large earthquakes measured from long-period Rayleigh waves. Phys Earth Planet Inter 52:56–84